Materials Science & Engineering A 801 (2021) 140414

Contents lists available at ScienceDirect

Materials Science & Engineering A

journal homepage: http://www.elsevier.com/locate/msea

Key roles of particles in grain refinement and material strengthening for an aluminum matrix composite

Jinfeng Nie [a,*], Yanfang Liu [a], Fang Wang [a], Hao Zhou [a], Yang Cao [a,**], Xiangfa Liu [b], Xianghai An [c], Xiaozhou Liao [c], Yuntian Zhu [d,e], Yonghao Zhao [a]

[a] Nano and Heterogeneous Materials Center, School of Materials Science and Engineering, Nanjing University of Science and Technology, Nanjing, 210094, China
[b] Key Laboratory for Liquid–Solid Structural Evolution and Processing of Materials, Ministry of Education, Shandong University, Jinan, 250061, China
[c] School of Aerospace, Mechanical and Mechatronic Engineering, The University of Sydney, Sydney, NSW, 2006, Australia
[d] Department of Materials Science and Engineering, City University of Hong Kong, Hong Kong, China
[e] School of Materials Science and Engineering, Southeast University, Nanjing, 211189, China

ARTICLE INFO

Keywords:
Composite
Ultrafine-grained materials
Plastic deformation
Hall-petch relationship
Particles

ABSTRACT

An aluminum matrix composite (AMC) containing ~5% TiB_2/TiC particles is processed by high-pressure torsion. The microstructures and mechanical properties of the composites are analyzed in detail. The processed AMC samples are compared to the corresponding monolithic matrix material to investigate the key roles of particles in grain refinement and material strengthening. It is found that a small portion of particles is beneficial for grain refinement while maintaining the integrity of the material. In addition, the presence of particles grants the ultrafine-grained AMC larger strain hardening capacity (energy storage capacity) than the ultrafine-grained aluminum.

1. Introduction

Aluminum matrix composites (AMCs) are important for automotive, aerospace and defense industries due to their high specific strength, excellent wear resistance, outstanding dimensional stability and superior damping capacity [1–4]. The key to the amazing properties of AMCs is the reinforcement particles. For example, the interfaces between particles and the matrix exert strong back-stress to the matrix [5], leading to back-stress strengthening [6]; homogeneous distribution of particles prevents the coalescence of micro-cracks and thus help avoiding premature failure of AMCs [7]. Manipulation with the particles is a very important practice to tailor the mechanical properties of AMCs, and has been one of the major focuses in the field of AMCs in the last 50 years [4,8].

It should be noted that metal matrices are the primary constituents of the AMCs, which also possess a strong potential for strengthening owing to the metallic nature. Grain refinement is an effective strategy for strengthening metallic materials [9]. Thanks to the fast development of severe plastic deformation (SPD) methods [10,11], extreme grain refinement to the ultrafine-grained regime and even the nanocrystalline regime is achievable nowadays [12]. Under SPD processing, grain refinement of AMCs undergoes complicated dislocation-particle interactions. The sizes, shapes, density and distribution of reinforcement particles all have significant effects on the microstructural evolution and grain refinement of AMCs [9,13]. For example, the steady state grain sizes of the matrix increase with decreasing particle sizes [14]. Notwithstanding, the role of reinforcement particles on grain refinement is case dependent. Qualitative experimental research is necessary to explain the effect of reinforcement particles on the grain refinement process.

It is known that uniform distribution of the reinforcement particles in the matrix and seamless integration between the reinforcement particles and matrix ameliorate the mechanical properties of AMCs [15–19]. In addition, SPD induced extreme grain refinement is capable of improving the strength of AMCs to a new high level [10,16,20–26]. SPD processed AMCs usually have complex microstructures consisting of high densities of dislocations, ultrafine-grained matrix structures and uniformly distributed particles [10,16,20]. Moreover, SPD processed AMCs may also contain micro-cracks, contaminated interphase interfaces, dissolved alloying elements and newly formed precipitates [27,28]. All of the

* Corresponding author.
** Corresponding author.
E-mail addresses: niejinfeng@njust.edu.cn (J. Nie), y.cao@njust.edu.cn (Y. Cao).

https://doi.org/10.1016/j.msea.2020.140414
Received 24 July 2020; Received in revised form 11 October 2020; Accepted 17 October 2020
Available online 21 October 2020

abovementioned microstructural features affect the mechanical properties of the AMCs. Hence, it is difficult to distinguish the effect of each microstructural feature on the mechanical properties of the SPD processed AMCs. However, it has been frequently claimed that the reinforcement particles have a substantial contribution to the strength of the SPD processed AMC [10,16,20–26], but to what extent has never been clarified.

HPT techniques can be classified into three types: constrained, quasi-constrained and unconstrained HPT [20]. The stress states in the samples processed by constrained and quasi-constrained HPT are very close to the ideal hydrostatic stress states, due to the lateral constraint. In addition, the lateral constraint generated by the depression wall can help keeping brittle materials intact by restricting lateral flow of materials [29–31]. Without the lateral constraint, large amounts of cracks or even crumbling of the bulk sample can occur for comparatively brittle materials such as metallic glass and metal matrix composites [31,32]. In case of processing AMCs, quasi-constrained HPT can impose very high strains without cracking the materials, thus to achieve extreme grain refinement [16]. Therefore, quasi-constrained HPT technique is chosen in the current experimental work.

2. Experimental procedure

In this work, an Al-3.6TiB_2-1.4TiC (namely Al-5%TiB_2/TiC in the following text) AMC ingot was fabricated by using an in-situ melt reaction method to ensure clear and seamless interfaces between the reinforcement particles and the matrix. The thermodynamic stabilities of interphase interfaces in the in-situ AMCs are generally better than those synthesized by exogenous fabrication processes [33,34]. Both TiC and TiB_2 are insoluble in Al, thus keeping the solid solution a constant parameter. The as-cast ingot was machined into disks with a diameter of ~10 mm and a thickness of ~1.7 mm. The disks were polished mechanically by using abrasive papers to a final thickness of ~1.4 mm for subsequent high-pressure torsion (HPT) processing. As illustrated in Fig. 1a, a disk sample is held between the massive anvils under the quasi-constrained condition with a pressure of 6.0 GPa. The bottom anvil rotates at a speed of 1 rpm to impose the plastic strain [35,36]. Disks were processed by HPT to 1, 2 and 5 turns at room temperature. The von Mises equivalent strain, ε_{eq}, imposed by HPT is expressed by the equation [20,37]:

$$\varepsilon_{eq} = \frac{2\pi rN}{\sqrt{3}h} \quad (1)$$

where r is the radius, N is the number of turns and h is the thickness of the disk.

During quasi-constrained HPT processing, a compressive load imposed by the anvils, a counter stress generated by the depression walls and the friction between the sample and the anvils cooperate simultaneously to create a huge hydrostatic stress in the sample material [29]. Although, the mean stress is usually calculated by dividing the compressive load in the anvils by the circular area of the disk, the actual stress state is in fact very complex. According to finite element analysis, the stress state at the disk center is close to the ideal compressive stress, the stress decreases gradually towards the periphery of the disk, creating a stress gradient in the bulk sample [29]. Nevertheless, local stress and strain imposed by HPT is very complicated; They are the fundamental reasons for the microscopic heterogeneity in HPT materials, and related research is still on-going [38].

Microstructures of the Al-5%TiB_2/TiC AMC samples were characterized by a Quanta-250F field emission gun scanning electron microscope (SEM) equipped with an Oxford energy dispersive X-ray spectrometer (EDS) and an electron backscattered diffraction (EBSD) detector, and a TECNAI-20 transmission electron microscope (TEM). Samples for SEM analysis were prepared by mechanical polishing with abrasive papers and fine polishing with Struers OP-U colloidal silica suspension. TEM samples were taken at the periphery regions and at the half-radius regions of the disks. TEM samples were prepared by ion beam thinning at 5 keV acceleration voltage and the beam angle of ~7° for perforation, and at 3 keV acceleration voltage and the beam angle of ~4° for final trimming.

Tensile tests were conducted at ambient temperature on a Walterbai-LFM-20kN universal test machine, with a strain rate of 5.6×10^{-4} s^{-1} to measure the strength of the as-cast and HPT samples. Dog-bone-shape tensile samples were cut by an electric discharge machine from HPT disks. As depicted in Fig. 1b, two tensile samples could be obtained from each disk, and the gauge section of the tensile sample is approximately at half radius of the disk.

3. Results

As shown by the SEM micrograph in Fig. 2a, the Al matrix in the as-cast sample has a coarse-grained (CG) microstructure (the average grain size of the Al matrix is ~59.8 μm, as confirmed by both SEM and EBSD analysis); TiC and TiB_2 particles with bright contrast assembled into clusters in the matrix. Clusters of particles are present at both grain interior and grain boundary (GB). Particle rich regions and particle free regions can be easily identified in the SEM image. After 1 turn and 2 turns of HPT, the GBs of the Al matrix are no longer identifiable in the SEM images shown Fig. 2b and **c**. However, the distribution of particle clusters is still similar to that shown in Fig. 2a. This is because the majority of the HPT imposed strain was accommodated by dislocation activities in the Al matrix and insufficient work was done to disassemble the particle clusters [16]. After 5 turns of HPT, the clusters were mostly disassembled and particles were homogeneously dispersed in the matrix at the location of approximately half-radius of the HPT disk, as shown in

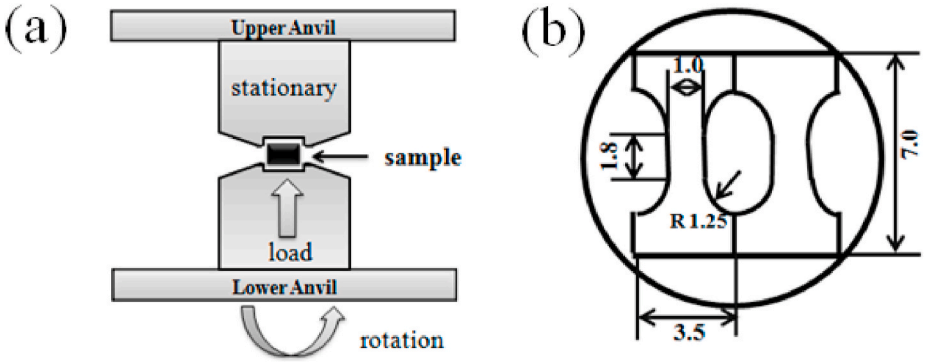

Fig. 1. (a) Schematic illustration of an HPT facility operating under the quasi-constrained condition, and (b) the dimensions of the tensile samples taken from an HPT disk.

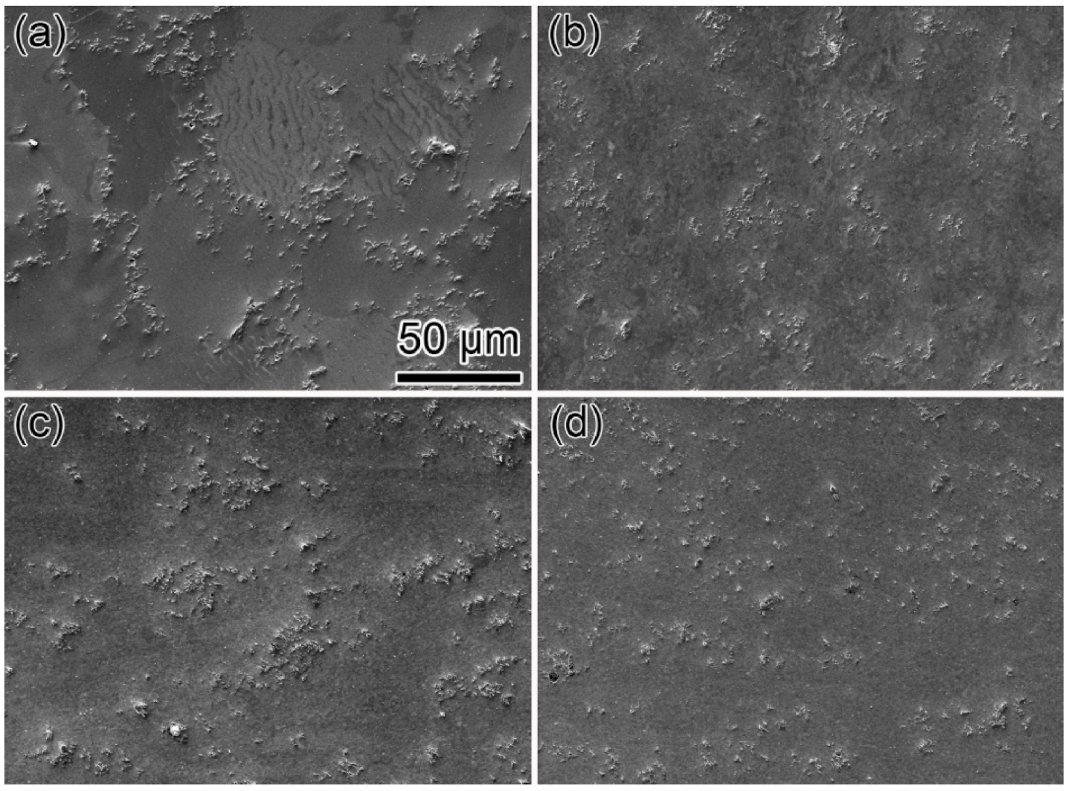

Fig. 2. (a) A SEM image showing the typical microstructure of the as-cast sample; SEM images showing microstructures at the half-radius regions of the disks processed to (b) 1 turn, (c) 2 turns and (d) 5 turns of HPT.

Fig. 2d.

Microstructures of the Al matrix processed by HPT were investigated in detail by TEM. As shown in Fig. 3a, after 1 turn HPT the grain sizes have been refined to an average of ~770 nm at the half-radius of the disk. Diffused dislocation boundaries can be frequently found, as indicated by yellow arrows in Fig. 3a, indicating that the grain refinement process is still in dominance. After 2 turns of HPT, the grain sizes were refined further to an average of ~636 nm at the half-radius of the disk, as shown in Fig. 3b. A high density of dislocation nodes appeared as dots with dark contrast can be seen at grain interiors, indicating that dislocation activities were still pronounced. After 5 turns of HPT, ultra-fine grains with an average size of ~387 nm at the half-radius of the disk

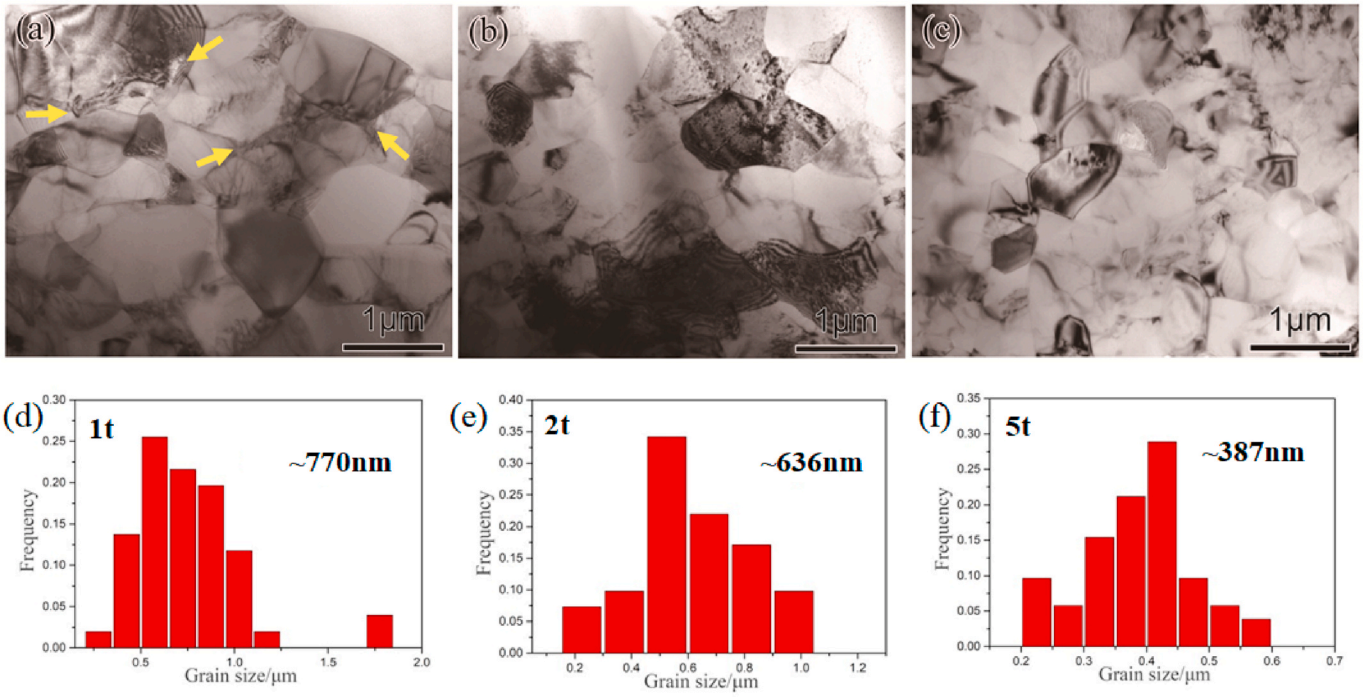

Fig. 3. TEM images showing typical microstructures at the half-radius regions of the disks processed by HPT for (a) 1 turn, (b) 2 turns and (c) 5 turns, and (d–f) the corresponding grain size distributions.

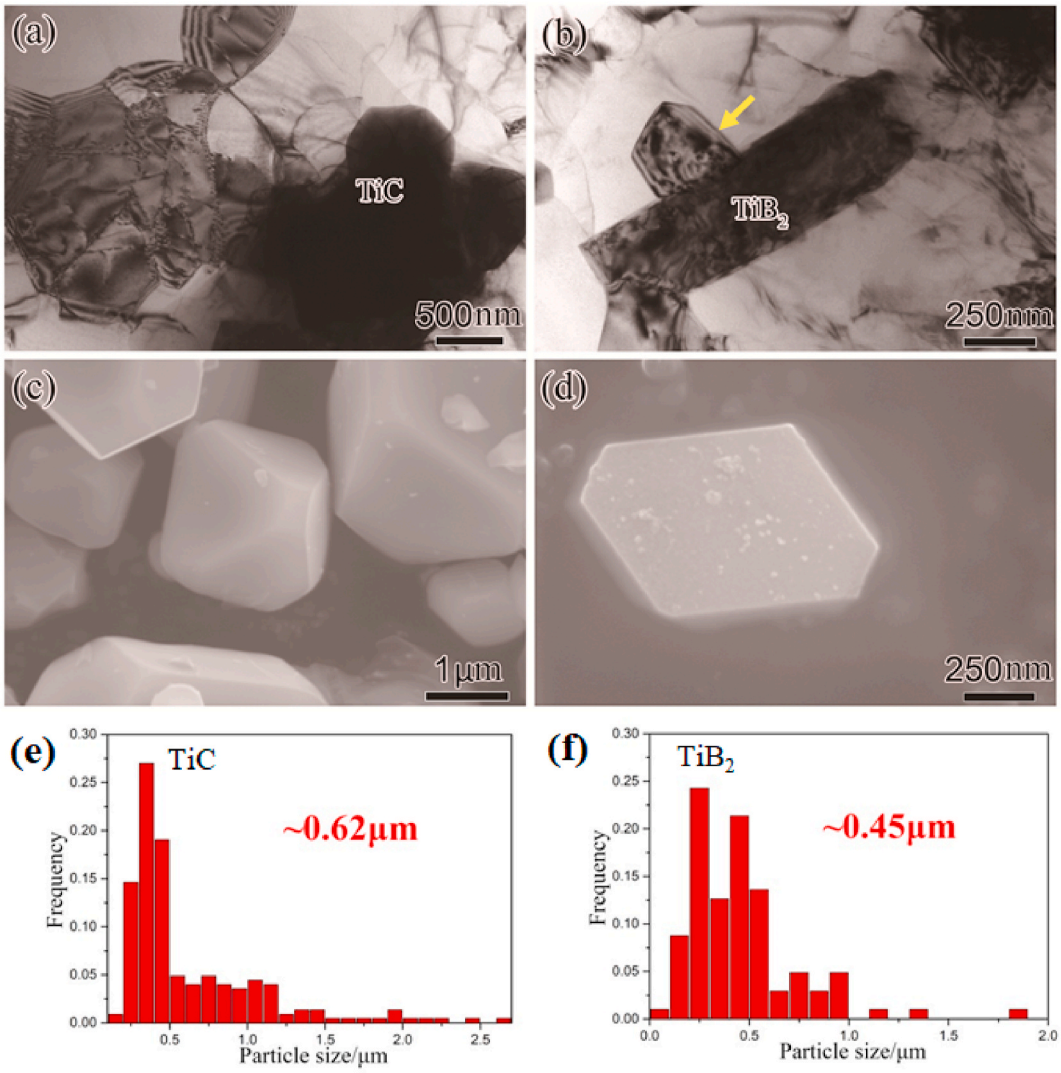

Fig. 4. TEM images showing (a) TiC particles and (b) TiB_2 particles embedded in the Al matrix of the 2-turn HPT sample; SEM images showing free-standing (c) TiC particles and (d) TiB_2 particles extracted from the as-cast Al-5%TiB_2/TiC AMC sample; Particle size distributions and the mean sizes of (e) TiC and (f) TiB_2 in the 2-turn HPT samples.

have been achieved, as shown in Fig. 3c. GBs are sharp and clear, dislocation debris are seldom found at grain interiors. Note that the average grain size at the half-radius of the 5-turn HPT disk is slightly smaller than the average size of ~446 nm at the periphery of the disk. This indicates that dynamic recovery and recrystallization have become very active when the equivalent strain is above ~30 (at the half-radius of the 5-turn HPT disk).

As shown in Fig. 4a andb, the TiC and TiB_2 particles are still seamlessly bonded to the matrix after 2 turns of HPT processing. As shown in Fig. 4b, a recrystallized Al grain with a sharp and smooth GB, marked by a yellow arrow, is adjacent to a TiB_2 particle, indicating that the local shear strain was sufficiently high to induced dynamic recrystallization.

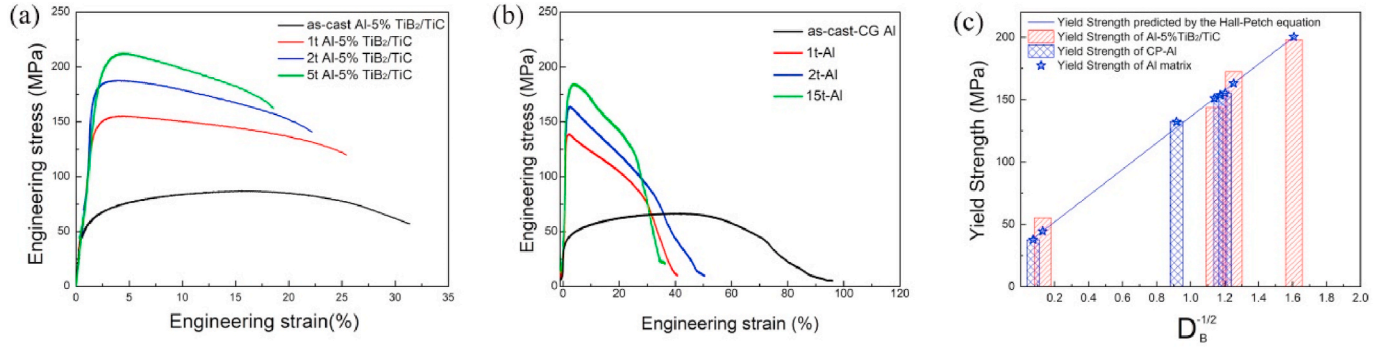

Fig. 5. (a) Engineering stress–strain behaviors for the as-cast and HPT Al-5%TiB_2/TiC AMCs; (b) Engineering stress–strain behaviors for coarse-grained CP-Al and HPT CP-Al; (c) Yield strength of sample materials and Hall-Petch relationship.

However, such a high shear strain did not tear open the interface between the TiB_2 particle and the Al matrix. Typical TiC and TiB_2 particles were extracted from the as-cast Al-5%TiB_2/TiC AMC sample. TiC particles shown in Fig. 4c are hexahedrons or polyhedrons of irregular shapes matching the 2D projection of the particle shown in Fig. 4a. TiB_2 particles shown in Fig. 4d are of platelet shapes matching the 2D projection of the particle shown in Fig. 4b. The TiC particles are generally of equiaxed shapes with an average crystal size of ~0.62 μm as shown in Fig. 4e. The TiB_2 particles have an average aspect ratio of ~3.4 and an average crystal size of ~0.45 μm (Fig. 4f). The high strength, small sizes and comparatively small aspect ratios make the TiC and TiB_2 particles unlikely to be broken by the shear strain transferred from the ductile Al matrix.

As shown in Fig. 5a, the as-cast Al-5%TiB_2/TiC AMC has a yield strength (YS) of ~55 MPa and a decent uniform elongation of 16.48%. After HPT processing to 1, 2 and 5 turns, the YS of the AMCs are improved to ~143 MPa, ~172 MPa, and ~198 MPa, respectively. The uniform elongations of 1-turn, 2-turn and 5-turn HPT samples are 2.24%, 1.66% and 2.91% respectively. Commercial purity Al (CP-Al, 99.7 wt%) samples, as reference materials, were processed by HPT to 1, 2 and 15 turns to obtain different grain sizes. Four CP-Al samples with different microstructures were tested by tensile deformation. The results are presented in Fig. 5b. The average grain sizes of the CG CP-Al, 1-turn HPT CP-Al, 2-turn HPT CP-Al and 15-turn HPT CP-Al are 185 μm, 1.187 μm, 0.725 μm and 0.692 μm, respectively. The YS of the CG CP-Al, 1-turn HPT CP-Al, 2-turn HPT CP-Al and 15-turn HPT CP-Al are ~37 MPa, ~132 MPa, ~153 MPa and ~155 MPa, respectively, as shown in Fig. 5b. The experimental data are collected in Table 1. The CG CP-Al has an excellent uniform elongation of 44.1%. In contrast, all the HPT CP-Al samples have uniform elongations in the range of 2%–4%. The results are reasonable that significant grain refinement induced by HPT can drastically improve the strength at the expense of ductility for most of the metallic materials [9,39].

The Al-5%TiB_2/TiC AMC used in the current work was fabricated by an in-situ melt reaction method, so the interphase interfaces between reinforcement particles and the matrix are similar to that between precipitates and the matrix, in terms of cohesive energy, coherency and integrity [3,17]. However, the yield strength of the Al-5%TiB_2/TiC AMC before and after HPT is significantly lower than many Al alloys, such as Al-2024 [40–42] and Al-7075 alloys [43]. This is because Al-2024 and Al-7075 alloys possess additional solid solution strengthening, nano-clusters strengthening and complicated precipitation strengthening effects in contrast to the Al-5%TiB_2/TiC AMC [40–43]. The purpose of this paper was not to seek highest strength in AMCs, but to specifically investigate the particle strengthening effect in ultrafine-grained AMCs. Ti, B, and C elements are insoluble in Al at room temperature. During the in-situ particle forming process, TiB_2 and TiC particles nucleated in the Al matrix, leaving the high purity Al matrix comparable to CP-Al. In other words, the composition and the intrinsic properties of the matrix of the in-situ Al-5%TiB_2/TiC AMC is very close to those of CP-Al. Thus, the only significant difference between the in-situ Al-5%TiB_2/TiC AMC and CP-Al is the presence of reinforcement particles. The strength of the matrix of the Al-5%TiB_2/TiC AMC and the strength of CP-Al are governed by the same parameters: the lattice friction stress (σ_0) which includes the contribution of solute atoms, the dislocation density (ρ_d) and the grain size (D_{GB}). The lattice friction stresses in both the matrix of the Al-5%TiB_2/TiC AMC and CP-Al are nearly the same due to analogous compositions. However, the dislocation density and grain size in both materials are variables affected the plastic strain and the presence of reinforcement particles [9]. During SPD, dislocation boundaries and sub-GBs are continuously formed. As a result, the grain sizes are significantly reduced, and the majorities of dislocations are accumulated at dislocation boundaries and sub-GBs. Thus, it is reasonable to estimate the YS of the material by the following Hall-Petch type equation [44]:

$$\sigma_y = \sigma_0 + \left[M\alpha_T G\sqrt{3b\theta_{LAB}(1-f)} + k_1\sqrt{f}\right]D_B^{-1/2} \quad (2)$$

where M is the mean orientation factor; α_T is a constant which has a temperature dependence; G is the shear modulus; b is the Burgers vector; $\theta_{LAB}$is the average misorientation angle of dislocation boundaries; $k_1$is the Hall-Petch constant for an undeformed polycrystalline metal; $f$is the density of high angle boundaries; D_B is the boundary spacing (both dislocation boundary and sub-GB). A complete derivation procedure for Eq. (2) is provided in the literature [44] by N. Hansen. The term $M\alpha_T G\sqrt{3b\theta_{LAB}(1-f)}$on the right-hand side of Eq. (2) accounts for the dislocation strengthening effect [9,45,46]. The term $k_1\sqrt{f}$accounts for the GB strengthening effect. The advantage of Eq. (2) is that the both dislocation strengthening effect and GB strengthening effect are trunked into one constant $k_2 = M\alpha_T G\sqrt{3b\theta_{LAB}(1-f)} + k_1\sqrt{f}$, which reflects the average effectiveness of all dislocation boundaries and sub-GBs in blocking dislocation slip. Therefore, Eq. (2) is simplified to:

$$\sigma_y = \sigma_0 + k_2 D_B^{-1/2} \quad (3)$$

The YS of CP-Al samples are plotted on Fig. 5c as blue columns with respect to the grain size. Let D_B equal to the average grain size of the CP-Al sample (under the diffraction contrast of TEM, dislocation boundaries and sub-GBs are similar, thus the grain sizes measured by TEM are usually equivalent to the boundary spacings). A linear fitting of the YS is estimated to be:

$$\sigma_y = 30.89 + 105.36\, D_B^{-1/2} \quad (4)$$

Therefore, $\sigma_0$and $k_2$for CP-Al are ~30.89 MPa and ~105.36 MPa/$\sqrt{\mu m}$, respectively. The value of $\sigma_0$is close to the theoretical value of 20 MPa, the value of $k_2$is within the theoretical range of 40–140 MPa/$\sqrt{\mu m}$ [44].

Under the assumption that the matrix material of the Al-5%TiB_2/TiC AMC is similar to CP-Al. The flow stress or YS of the matrix can be estimated by substituting the TEM measured grain sizes into Eq. (4). The estimated YS of the matrix are marked by blue stars on the red columns. The red columns are the YS of the Al-5%TiB_2/TiC AMC samples obtained

Table 1
Mechanical properties of sample materials (the stored energy is calculated from true stress-strain curves).

Samples	Average grain size for Al (μm)	Yield Strength (MPa)	Ultimate Tensile Strength (MPa)	Uniform Elongation (%)	Stored Energy (J/g)
as-cast Al-5%TiB_2/TiC	59.8	55.2	87.3	16.48	2.2500
1-turn HPT Al-5%TiB_2/TiC	0.77	143.6	155.4	2.24	0.5141
2-turns HPT Al-5%TiB_2/TiC	0.63	172.4	187.2	1.66	0.2982
5-turns HPT Al-5%TiB_2/TiC	0.38	198.1	212.2	2.91	0.2424
CP-Al	185	37.5	66.5	44.1	8.9898
1-turn HPT CP-Al	1.187	132.2	138.3	2.23	0.0530
2-turns HPT CP-Al	0.725	153.6	163.4	2.50	0.0253
15-turns HPT CP-Al	0.692	155.1	184.0	3.97	0.0124

by tensile tests. The as-cast Al-5%TiB_2/TiC AMC has a YS of ~55 MPa that is 24% higher than the estimated YS of the matrix (~44 MPa). Clearly the reinforcement particles are very effective in strengthening the as-cast Al-5%TiB_2/TiC AMC with coarse grains. However, for the HPT processed Al-5%TiB_2/TiC AMC samples, the YS of the Al-5%TiB_2/TiC AMC is not superior to the YS of the matrix alone. As illustrated in Fig. 5c, the YS of the Al-5%TiB_2/TiC AMCs processed to 1 turn and 5 turns of HPT are somehow 4.8% and 1% lower than the strength of the corresponding matrices. For the 2-turn HPT sample, the YS of the Al-5%TiB_2/TiC AMC is only 5.7% higher than the YS of the matrix. The result indicates that the contribution of the reinforcement particles to the flow stress is negligible in the HPT processed Al-5%TiB_2/TiC AMCs.

4. Discussion

One may argue that SPD induced micro-cracks and delamination of particles may deteriorate the strength of the composite and offset the particle strengthening effect. However, as shown in Fig. 2 there is no obvious increase for extent of micro-cracks after HPT processing. As shown in Fig. 4a and **b**, the reinforcement particles are still seamlessly bonded to the matrix after HPT processing. In addition, the ductility of the HPT AMCs and HPT CP-Al are comparable. Thus, the SPD induced micro-cracks and delamination of particles are considered negligible. In fact, micro-cracks and delamination of particles often form in AMCs containing high densities of particles and/or large particles with sizes in the micrometer range or larger [7,27]. The volume fraction of particles is low (~5%) in the present AMC sample and the size and aspect ratios of the particles are comparatively small. Thus, micro-cracks and delamination of particles are minimized in the experiment.

As SPD induced micro-cracks and delamination of particles are negligible, the decreased particle strengthening effect reflected by Fig. 5c is now considered rational. It is known that the particle strengthening effect in conventional CG AMCs is mainly due to the Orowan mechanism [9,13]. The particles scattered at the grain interiors (as shown in Fig. 2a) act as obstacles to dislocation slip, in addition to dislocation boundaries and GBs. In other words, the presence of particles at the grain interior significantly reduces the mean free path for dislocation slip. However, it can be seen that after HPT processing the matrix grain sizes are comparable and even smaller than the particle sizes, by comparing the grain sizes and particle sizes in Figs. 3 and 4. Thus, the Orowan mechanism is no longer operative during tensile deformation. The particle-matrix interfaces in the ultrafine-grained AMCs act more like ordinary GBs. Therefore, it is concluded that the absence of Orowan mechanism and the ultrafine grain sizes are the cause of the ineffective particle strengthening effect.

However, the particles have significantly higher Young's modulus than the Al matrix, leading to a high image force [9] and strong back-stress [6] at the interphase interface. Thus, higher dislocation storage capacity and stronger back-stress strengthening effect is still expected in the Al-5%TiB_2/TiC AMC than CP-Al, in despite of the ultrafine grains. According to the work of Wiera and Michał, the energy stored by non-homogeneous plastic deformation can be estimated from a true stress-strain curve by the equation [47]:

$$e_s = w_p - q - e_{te} \tag{5}$$

where w_p is the mechanical energy expended on plastic deformation, q is the energy dissipated as heat, and e_{te} is the isentropic energy [48]. The energy stored by non-homogeneous plastic deformation is a sum of the lattice stretch energy, energy of geometrically necessary dislocations and energy of long-range internal stresses due to heterogeneous distribution of dislocations. In other words, e_s is the energy stored due to hetero-deformation at the microscale [6]. In ultrafine-grained materials, non-homogeneous plastic deformation account for the majority of the plastic strain, due to enormous amounts of boundaries. Thus, e_s can be used for comparing the energy storage capacities of materials. CG CP-Al has a e_s of 8.9898 J/g, reflecting a very strong strain hardening effect and a huge energy storage capacity. After HPT processing to 1-turn, the e_s of CP-Al is drastically reduced to 0.0530 J/g. In contrast, the as-cast Al-5%TiB_2/TiC AMC has a e_s of 2.25 J/g; After HPT processing to 5 turns, its e_s is reduced to 0.2424 J/g, but still significantly higher than the HPT CP-Al. (The values of e_s for all samples are provided in Table 1.) Therefore, ultrafine-grained Al-5%TiB_2/TiC AMC has a significantly better energy storage capacity than the corresponding monolithic matrix material.

5. Conclusions

In summary, the presence of a small portion (~5%) of ultrafine reinforcement particles in the Al-5%TiB_2/TiC AMC can significantly improve the strength of the as-cast sample. After HPT processing, the steady state grain size of the matrix of Al-5%TiB2/TiC AMC is significantly smaller than that of the CP-Al, and micro-cracks and delamination of particles are negligible, indicating that a small portion of particles is beneficial for grain refinement while keeping the integrity of the material. The YS of HPT AMCs lay on the same Hall-Petch type slope of the HPT CP-Al samples, indicating that the particle strengthening effect is minimized or ineffective in the ultrafine-grained matrix in absence of the Orowan mechanism. Notwithstanding, during plastic deformation ultrafine-grained AMCs show better energy storage capacity than ultrafine-grained CP-Al, indicating the strong back-stress strengthening effect due to the presence of non-deformable particles. Our result suggests that the particle strengthening effect is better utilized when both Orowan strengthening and boundary strengthening are in effect. In absence of the Orowan mechanism, the particles can still exert back-stress to dislocation slip due to image force and high boundary strength to cause back-stress strengthening.

Data availability

All data included in this study are available upon request by contact with the corresponding author.

CRediT authorship contribution statement

Jinfeng Nie: Conceptualization, Investigation, Writing - review & editing. **Yanfang Liu:** Investigation, Data curation. **Fang Wang:** Investigation, Writing - original draft, Data curation. **Hao Zhou:** Formal analysis. **Yang Cao:** Conceptualization, Investigation, Writing - review & editing. **Xiangfa Liu:** Supervision, Formal analysis. **Xianghai An:** Methodology, Formal analysis. **Xiaozhou Liao:** Methodology, Formal analysis. **Yuntian Zhu:** Supervision, Writing - review & editing. **Yonghao Zhao:** Supervision, Writing - review & editing.

Declaration of competing interest

The authors declare that they have no known competing financial interests for personal relationships that could have appeared to influence the work reported in this paper.

Acknowledgements

This work is supported by the National Key R&D Program of China (2017YFA0204403), National Natural Science Foundation of China (51731007, 52071179, 52071181, 51971112 and 51931003), the Fundamental Research Funds for the Central Universities (Nos. 30920021160 and 30919011405). and Australian Research Council (DP190102243). The authors are thankful for the technical support from Jiangsu Key Laboratory of Advanced Micro&Nano Materials and Technology and the Materials Characterization Facility of Nanjing University of Science and Technology. The authors acknowledge the delightful discussion with Prof. Shuang Li.

References

[1] A.J. Trowsdale, B. Noble, S.J. Harris, I.S.R. Gibbins, G.E. Thompson, G.C. Wood, Corrosion Sci. 38 (1996) 177–191.
[2] J.S. Moya, S. Lopez-Esteban, C. Pecharromán, Prog. Mater. Sci. 52 (2007) 1017–1090.
[3] R. Anandkumar, A. Almeida, R. Vilar, Surf. Coating. Technol. 205 (2011) 3824–3832.
[4] L.J. Huang, L. Geng, H.X. Peng, Prog. Mater. Sci. 71 (2015) 93–168.
[5] T. Mori, T. Mura, Acta Metall. 26 (1978) 1199–1204.
[6] Y. Zhu, X. Wu, Mater. Res. Lett. 7 (2019) 393–398.
[7] J. Llorca, Prog. Mater. Sci. 47 (2002) 283–353.
[8] M.F. Ashby, Acta Metall. Mater. 41 (1993) 1313–1335.
[9] Y. Cao, S. Ni, X. Liao, M. Song, Y. Zhu, Mater. Sci. Eng. R Rep. 133 (2018) 1–59.
[10] Y. Huang, P. Bazarnik, D. Wan, D. Luo, P.H.R. Pereira, M. Lewandowska, J. Yao, B. E. Hayden, T.G. Langdon, Acta Mater. 164 (2019) 499–511.
[11] Y. Liu, M. Liu, X. Chen, Y. Cao, H.J. Roven, M. Murashkin, R.Z. Valiev, H. Zhou, Scripta Mater. 159 (2019) 137–141.
[12] X.H. An, S.D. Wu, Z.G. Wang, Z.F. Zhang, Prog. Mater. Sci. 101 (2019) 1–45.
[13] C.L. Li, Q.S. Mei, J.Y. Li, F. Chen, Y. Ma, X.M. Mei, Scripta Mater. 153 (2018) 27–30.
[14] Y.F. Shen, R.G. Guan, Z.Y. Zhao, R.D.K. Misra, Acta Mater. 100 (2015) 247–255.
[15] Y.H. Zhao, X.Z. Liao, S. Cheng, E. Ma, Y.T. Zhu, Adv. Mater. 18 (2006) 2280–2283.
[16] Y. Liu, F. Wang, Y. Cao, J. Nie, H. Zhou, H. Yang, X. Liu, X. An, X. Liao, Y. Zhao, Y. Zhu, Scripta Mater. 162 (2019) 316–320.
[17] M.W. Finnis, J. Phys. Condens. Matter 8 (1996) 5811–5836.
[18] P. Xiao, B. Derby, Acta Mater. 44 (1996) 307–314.
[19] S.V. Dudiy, B.I. Lundqvist, Phys. Rev. B 69 (2004), 125421.
[20] A.P. Zhilyaev, T.G. Langdon, Prog. Mater. Sci. 53 (2008) 893–979.
[21] H. Zare, M. Jahedi, M.R. Toroghinejad, M. Meratian, M. Knezevic, Mater. Sci. Eng. A 670 (2016) 205–216.
[22] I. Sabirov, O. Kolednik, R.Z. Valiev, R. Pippan, Acta Mater. 53 (2005) 4919–4930.
[23] H. Zare, M. Jahedi, M.R. Toroghinejad, M. Meratian, M. Knezevic, Mater. Des. 106 (2016) 112–119.
[24] P. Quang, Y.G. Jeong, S.C. Yoon, S.H. Hong, H.S. Kim, J. Mater. Process. Technol. 187–188 (2007) 318–320.
[25] J.F. Nie, F. Wang, Y.S. Li, Y. Cao, X.F. Liu, Y.H. Zhao, Y.T. Zhu, Materials 10 (2017) 13.
[26] M. Alizadeh, H.A. beni, M. Ghaffari, R. Amini, Mater. Des. 50 (2013) 427–432.
[27] S.J. Huang, A.N. Ali, J. Mater. Process. Technol. 272 (2019) 28–39.
[28] M. Jahedi, M.H. Paydar, M. Knezevic, Mater. Char. 104 (2015) 92–100.
[29] R.B. Figueiredo, P.R. Cetlin, T.G. Langdon, Mater. Sci. Eng. A 528 (2011) 8198–8204.
[30] K. Edalati, I. Fujita, X. Sauvage, M. Arita, Z. Horita, J. Alloys Compd. 779 (2019) 394–398.
[31] Y.B. Wang, D.D. Qu, X.H. Wang, Y. Cao, X.Z. Liao, M. Kawasaki, S.P. Ringer, Z. W. Shan, T.G. Langdon, J. Shen, Acta Mater. 60 (2012) 253–260.
[32] G. Ramu, R. Bauri, Mater. Des. 30 (2009) 3554–3559.
[33] M. Emamy, M. Mahta, J. Rasizadeh, Compos. Sci. Technol. 66 (2006) 1063–1066.
[34] J.F. Nie, F. Wang, Y.S. Li, Y.F. Liu, X.F. Liu, Y.H. Zhao, Trans. Nonferrous Metals Soc. China 27 (2017) 2548–2554.
[35] R.B. Figueiredo, P.H.R. Pereira, M.T.P. Aguilar, P.R. Cetlin, T.G. Langdon, Acta Mater. 60 (2012) 3190–3198.
[36] X.H. An, Q.Y. Lin, G. Sha, M.X. Huang, S.P. Ringer, Y.T. Zhu, X.Z. Liao, Acta Mater. 109 (2016) 300–313.
[37] Y. Cao, Y.B. Wang, R.B. Figueiredo, L. Chang, X.Z. Liao, M. Kawasaki, W.L. Zheng, S.P. Ringer, T.G. Langdon, Y.T. Zhu, Acta Mater. 59 (2011) 3903–3914.
[38] W. Jiang, H. Zhou, Y. Cao, J. Nie, Y. Li, Y. Zhao, M. Kawasaki, T.G. Langdon, Y. Zhu, Adv. Eng. Mater. 22 (2020), 1900477.
[39] I.A. Ovid'ko, R.Z. Valiev, Y.T. Zhu, Prog. Mater. Sci. 94 (2018) 462–540.
[40] S.V. Dobatkin, E.N. Bastarache, G. Sakai, T. Fujita, Z. Horita, T.G. Langdon, Mater. Sci. Eng. A 408 (2005) 141–146.
[41] M. Liu, R. Zheng, J. Li, C. Ma, Mater. Sci. Eng. A 788 (2020), 139576.
[42] A. Alhamidi, Z. Horita, Mater. Sci. Eng. A 622 (2015) 139–145.
[43] P.V. Liddicoat, X.Z. Liao, Y. Zhao, Y. Zhu, M.Y. Murashkin, E.J. Lavernia, R. Z. Valiev, S.P. Ringer, Nat. Commun. 1 (2010) 63.
[44] N. Hansen, Scripta Mater. 51 (2004) 801–806.
[45] U.F. Kocks, H. Mecking, Prog. Mater. Sci. 48 (2003) 171–273.
[46] K. Ma, H. Wen, T. Hu, T.D. Topping, D. Isheim, D.N. Seidman, E.J. Lavernia, J. M. Schoenung, Acta Mater. 62 (2014) 141–155.
[47] W. Oliferuk, M. Maj, Eur. J. Mech. Solid. 28 (2009) 266–272.
[48] A. Chrysochoos, O. Maisonneuve, G. Martin, H. Caumon, J.C. Chezeaux, Nucl. Eng. Des. 114 (1989) 323–333.